THE DYNAMICAL MASS AND THREE-DIMENSIONAL ORBIT OF HR7672B: A BENCHMARK BROWN DWARF WITH HIGH ECCENTRICITY

JUSTIN R. CREPP[1], JOHN ASHER JOHNSON[1,2], DEBRA A. FISCHER[3], ANDREW W. HOWARD[4], GEOFFREY W. MARCY[4],
JASON T. WRIGHT[5,6], HOWARD ISAACSON[4], TABETHA BOYAJIAN[7,8], KASPAR VON BRAUN[2], LYNNE A. HILLENBRAND[1],
SASHA HINKLEY[1,9], JOHN M. CARPENTER[1], AND JOHN M. BREWER[3]

[1] Department of Astrophysics, California Institute of Technology, 1200 E. California Blvd., Pasadena, CA 91125, USA; jcrepp@astro.caltech.edu
[2] NASA Exoplanet Science Institute, California Institute of Technology, MC 100-22, Pasadena, CA 91125, USA
[3] Department of Physics, Yale University, New Haven, CT 06511, USA
[4] Department of Astronomy, University of California, Berkeley, CA 94720, USA
[5] Department of Astronomy & Astrophysics, The Pennsylvania State University, University Park, PA 16802, USA
[6] Center for Exoplanets and Habitable Worlds, The Pennsylvania State University, University Park, PA 16802, USA
[7] Center for High Angular Resolution Astronomy, Department of Physics and Astronomy, Georgia State University, Atlanta, GA 30302, USA

ABSTRACT

The companion to the G0V star HR7672 directly imaged by Liu et al. has moved measurably along its orbit since the discovery epoch, making it possible to determine its dynamical properties. Originally targeted with adaptive optics because it showed a long-term radial velocity (RV) acceleration (trend), we have monitored this star with precise Doppler measurements and have now established a 24 year time baseline. The RV variations show significant curvature (change in the acceleration) including an inflection point. We have also obtained a recent image of HR7672B with NIRC2 at Keck. The astrometry also shows curvature. In this paper, we use jointly fitted Doppler and astrometric models to calculate the three-dimensional orbit and dynamical mass of the companion. The mass of the host star is determined using a direct radius measurement from CHARA interferometry in combination with high-resolution spectroscopic modeling. We find that HR7672B has a highly eccentric, $e = 0.50^{+0.01}_{-0.01}$, near edge-on, $i = 97.3^{+0.4}_{-0.5}$ deg, orbit with semimajor axis, $a = 18.3^{+0.4}_{-0.5}$ AU. The mass of the companion is $m = 68.7^{+2.4}_{-3.1} \, M_J$. HR7672B thus resides near the substellar boundary, just below the hydrogen-fusing limit. These measurements of the companion mass are independent of its brightness and spectrum and establish HR7672B as a rare and precious "benchmark" brown dwarf with a well-determined mass, age, and metallicity essential for testing theoretical evolutionary models and synthetic spectral models. Indeed, we find that such models under-predict its luminosity by a factor of ≈ 2. HR 7672B is presently the only L, T, or Y dwarf known to produce an RV trend around a solar-type star.

Key words: astrometry – brown dwarfs – techniques: high angular resolution – techniques: interferometric – techniques: spectroscopic

Online-only material: color figures

1. INTRODUCTION

Brown dwarfs have complicated atmospheres. Unlike stars, for which it is possible to infer bulk physical properties from spectra alone, the emergent radiation from substellar objects is currently not well understood (e.g., Cushing et al. 2008). More than a decade following the direct detection of the first L and T dwarfs (Becklin & Zuckerman 1988; Nakajima et al. 1995; Oppenheimer et al. 1995; Rebolo et al. 1995; Basri et al. 1996; Kirkpatrick et al. 1999b), and now faced with the recent detection of the first Y dwarfs (Cushing et al. 2011; Liu et al. 2011; Luhman et al. 2011), theoretical spectral models are still undergoing major developments as they presently do not capture all of the relevant physics involved in shaping the spectra of cold bodies (Allard et al. 1997; Marley et al. 2002; Baraffe et al. 2003; Burrows et al. 2006; Saumon & Marley 2008).

Factors that complicate the interpretation of brown dwarf spectra include the necessity to simultaneously model: the opacity of molecular species having millions of absorption lines, which results in an ill-defined continuum; the formation and settling of dust grains; non-equilibrium chemistry resulting from convective mixing; and temporal changes from weather patterns, among other phenomena (Cushing et al. 2008; Marley et al. 2010). Furthermore, the basic model input parameters, such as mass, radius, age, metallicity, and effective temperature, are often degenerate with one another, particularly for the faintest objects for which only broadband photometry or low-resolution spectroscopy are available (Dupuy et al. 2009a; Janson et al. 2011; Galicher et al. 2011). In order to improve our understanding of low-temperature atmospheres and guide the development of more sophisticated models, it is necessary to measure one or more of these physical properties independently of spectra and photometry.

Substellar companions found orbiting nearby stars serve as useful laboratories for calibrating theoretical models. Properties of the host star are more readily measured and may be used to infer those of the companion, such as chemical composition or possibly age, under the assumption that the star and brown dwarf formed from the same material at the same time (Pinfield et al. 2006). A number of these "benchmark" systems have recently been discovered (Lane et al. 2001; Close et al. 2005; Liu et al. 2007; Ireland et al. 2008; Dupuy et al. 2009a; Bowler et al. 2009; Biller et al. 2010; Wahhaj et al. 2011).

It is also possible to measure the *mass* of brown dwarfs (and extrasolar planets) using orbital dynamics. This has been accomplished in the past using the transit technique in combination

---

[8] Hubble Fellow.
[9] Sagan Fellow.

with Doppler radial velocity (RV) observations (Stassun et al. 2006; Johnson et al. 2011a). However, substellar companions with large semimajor axes and proximate distances may be imaged directly (spatially resolved from their host) using adaptive optics (AO) and high-contrast imaging technology (Marois et al. 2006; Oppenheimer & Hinkley 2009; Absil & Mawet 2010; Crepp et al. 2011). The companion sky-projected orbit can then be traced by measuring its position relative to the star over multiple epochs. This type of astrometry has been used for decades to characterize the orbits of binary stars (Aitken 1919) and is significantly easier to realize in practice compared to monitoring the "wobble" of a star in the sky relative to an inertial reference grid with <0.1 mas accuracy.

If Doppler measurements of the primary star are also obtained over a comparable time baseline, one can construct a three-dimensional orbit. Since the astrometry breaks the $sin(i)$ inclination degeneracy resulting from RV measurements alone, a Keplerian model that self-consistently combines both data sets provides an estimate of the companion true mass (e.g., Boden et al. 2006). Knowing the mass of non-hydrogen-fusing objects is crucial because it governs their luminosity evolution in time (Stevenson 1991; Burrows et al. 1997).

It is commonly thought that the long orbital periods of wide-separation companions prohibit the calculation of dynamical masses. However, those with semimajor axes as large as $a \approx 30$ AU orbiting nearby ($d \lesssim 100$ pc) stars may be characterized in several years to tens of years, because the size of the astrometric uncertainties are ~1–2 orders of magnitude smaller than the size of the orbit on the sky (thanks in part to the recent miniaturization in the physical size of detector pixels). Orbital solutions converge when both the astrometry and RVs become "unique," which generally corresponds to showing curvature or a change in the acceleration (also known as the "jerk").[10] With accuracies of ≈10 mas (e.g., the size of a pixel in the NIRC2 camera at Keck—PI: Keith Matthews), it is possible to calculate the inclination, as well as other parameters, in only several tenths of an orbital phase wrap (tens of degrees change in the true anomaly) depending on the orbit orientation and observing dates (Konopacky et al. 2010; Currie et al. 2011; Dupuy & Liu 2011). The constraints become tighter with time as the companion executes its motion along the ellipse.

A natural method to identify promising high-contrast imaging targets is to select stars that show long-term Doppler accelerations (trends). This approach is convenient because RV programs have now established time baselines exceeding a decade. For example, the L4.5 ± 1.5 dwarf companion to HR7672 (=Gl 779, =HD190406) was discovered by Liu et al. (2002) using this technique. This G0V star was originally chosen for AO observations because it showed unambiguous evidence for the existence of a distant companion with substellar minimum mass: an ≈ -24 m s^{-1} yr^{-1} acceleration over a 14 year baseline. HR7672B is currently the only L, T, and Y dwarf known to produce an RV trend around a solar-type star.

In this paper, we present an updated RV time series that shows significant orbital motion of the companion since the epoch of the direct imaging discovery. We have also obtained a new astrometric measurement with NIRC2 at Keck. Combining our observations with astrometry from the literature, and

performing a joint-fit analysis to the full data set, we construct a three-dimensional orbit and calculate the dynamical mass of HR7672B with a fractional error of only 4% using Newtonian dynamics. By explicitly connecting the mass of a brown dwarf to its radiative properties, the results may be used to inform both theoretical evolutionary models and synthetic spectral models. This study is afforded by an equally detailed characterization of HR7672A, for which we have modeled its high-resolution spectrum to determine its surface gravity and metallicity, acquired a spectral energy distribution (SED) to determine its luminosity, and measured its radius directly using interferometry, which also helps determine its mass.

2. OBSERVATIONS

2.1. Doppler Measurements

HR7672 was initially observed with the 0.6 m Coude Auxiliary Telescope (CAT) at Lick Observatory on 1987 September 9 UT. Several years of observations using the CAT, as well as the Lick 3 m (Hamilton)—both of which feed the Coude echelle spectrograph—revealed the star to have a linear RV trend (Cumming et al. 1999). We also began Doppler monitoring of this star at Keck on 1997 June 2 UT using the HIgh-Resolution Echelle Spectrometer (HIRES; Vogt et al. 1994). For each instrument, we used the iodine cell referencing method to measure precise RVs (Marcy & Butler 1992; Butler et al. 1996). Both data sets showed a consistent long-term acceleration. When Liu et al. (2002) targeted this star with AO, finding that indeed a low-mass companion with a wide orbit was responsible for the trend, there was very little, if any, perceptible change in the acceleration.

We have continued to monitor HR7672 at both Lick and Keck Observatories and have now established a 24 year time baseline. Our most recent RV data reveal significant curvature, making it possible to place tight constraints on the companion orbit. When combined with astrometry, this information is sufficient to converge to a unique orbital solution and companion mass, despite having coverage over a fraction of a single orbit cycle, because the signal-to-noise ratio in both data sets is high.

2.2. Astrometry from High-contrast Imaging

HR7672B has been imaged several times since its discovery. In 2002 July, Boccaletti et al. (2003) detected the companion with PHARO (Hayward et al. 2001) at Palomar in each of the J, H, and K_s bands to obtain color information and validate the spectral type assigned by Liu et al. (2002) from K-band spectroscopy. In 2006 September, Serabyn et al. (2009) observed HR7672B at Palomar to demonstrate the feasibility of new coronagraphic technologies and the use of "extreme" AO. Both studies reported astrometric measurements of the position of HR7672B relative to the primary. We have also retrieved Very Large Telescope (VLT) archival images of the system from 2007 September (PI: A. Boccaletti—program ID 279.C-5052(A)). These observations show clear orbital motion in a clockwise direction (north up, east left) when combined with the Liu et al. (2002) results.

We obtained additional images of HR7672B on 2011 May 15 using the Keck AO system with NIRC2. Given the large flux ratio between the primary and companion, we used the 300 mas diameter coronagraphic occulting spot to permit relatively long exposures without saturating the detector. The spot is partially transmissive and thus allows us to accurately measure the companion separation and position angle. Our initial

---

[10] See Lu et al. (2009) for analysis of an equivalent problem involving stars orbiting the supermassive black hole in the center of the Galaxy. The orbits are well characterized even though the periods are of the order of thousands of years. Likewise, the orbits of comets residing in the outer solar system may be determined with a time baseline of only several days (Bernstein & Khushalani 2000).
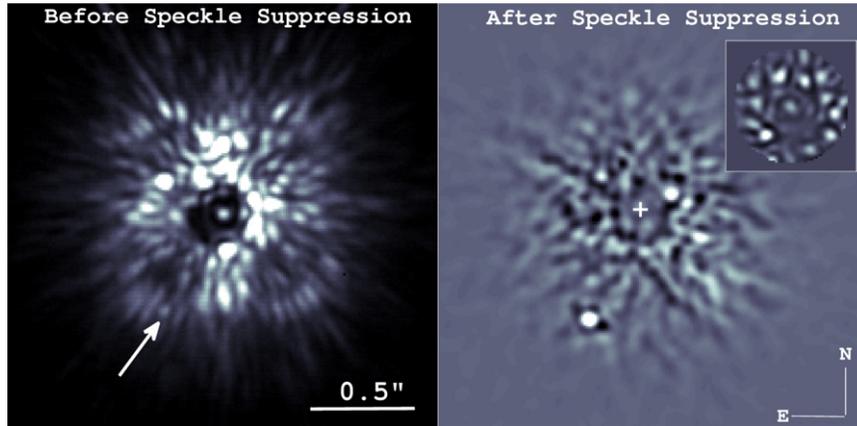
Figure 1. Direct image of HR7672B in the K' filter taken on 2011 May 15 UT with NIRC2 at Keck. Left: single image prior to PSF subtraction. The companion is located inside of the quasi-static speckle halo though discernible in individual frames. Right: processed image using the ADI technique and LOCI algorithm. The companion is detected at 36σ with 450 s of integration time. The inset subimage displays a cutout of the central region when our speckle suppression algorithm uses all available ADI frames but avoids PSF subtraction over the coronagraphic spot. The stellar Airy pattern is clearly visible facilitating astrometric measurements. We use data sets both with and without PSF subtraction to calculate the companion position relative to the star. This most recent observation increases the astrometric time baseline by 3.6 years.

(A color version of this figure is available in the online journal.)

Table 1
Astrometry Measurements Used for Orbital Analysis

Year	JD$-$2,440,000	ρ (mas)	P.A. ($^\circ$)	Instrument	Reference
2001.64	12144	786 ± 6	157.9 ± 0.5	NIRC2	Liu et al. (2002)
2001.94	12254	794 ± 5	157.3 ± 0.6	NIRC2	Liu et al. (2002)
2002.54	12473	788 ± 6	156.6 ± 0.9	PHARO	Boccaletti et al. (2003)
2006.69	13989	750 ± 80	155.0 ± 5.0	PHARO	Serabyn et al. (2009)
2007.73	14367	742 ± 35	151.8 ± 2.9	NACO	Program 279.C-5052(A)
2011.37	15697	519 ± 6	147.1 ± 0.5	NIRC2	Present study

data set consisted of 20 frames recorded using the narrow camera in position-angle mode (15 with the K' filter and 5 with the H filter). Although difficult to identify in a single exposure without prior knowledge of its approximate location, the majority of our raw frames did reveal the companion (Figure 1).

To further isolate the signal of HR7672 B from residual scattered starlight, we also obtained a 30 frame sequence with the K' filter using the angular differential imaging (ADI) technique (Marois et al. 2006). The parallactic angle changed by $12\overset{\circ}{.}7$ during this second sequence of images, providing sufficient angular diversity to remove the speckles and keep light from the companion (Lafrenière et al. 2007). Figure 1 displays our high-contrast images before and after speckle suppression.

We measured the position of HR7672B relative to the primary star in each data set (K' without ADI, H without ADI, and K' with ADI). The companion and stellar point-spread function (PSF) core were fitted with a Gaussian function using a least-squares iteration to find the astrometric centroid position in each processed frame. We correct for differential geometric distortion (warping) using the publicly available code provided by the Keck NIRC2 astrometry support Web site. Adopting a plate scale value of 9.963 ± 0.006 mas pixel^{-1} and instrument orientation relative to the sky of $0\overset{\circ}{.}13 \pm 0\overset{\circ}{.}02$ east of north, as measured by Ghez et al. (2008), we find a companion separation and position angle of 519 ± 6 mas and $147.1 \pm 0\overset{\circ}{.}5$, respectively.[11] HR7672B orbits in a clockwise direction and is

now significantly closer to its host star compared to the discovery epoch.

To estimate the uncertainty in our measurements, we calculate the standard deviation in the position resulting from each data set. We include a characteristic 5 mas error to account for astrometric bias introduced by the coronagraphic spot (Q. M. Konopacky 2011, private communication). This error is added in quadrature with the uncertainty from the plate scale and instrument orientation. The results were combined using a weighted average to determine the final uncertainties. We find that the measurements from each data set are consistent with one another to within the (1σ) error bars. Simulated companions were injected into the images and their positions recovered to validate our results. Table 1 lists the separation and position angles used for our three-dimensional orbit analysis.[12]

2.3. Physical Properties of the Host Star

The mass of the companion is tied to the mass of the primary star through the RV semi-amplitude and Kepler's equation. Astrometry determines the system total mass, and Doppler measurements can break the degeneracy between the system total mass and individual masses. However, we only have precise Doppler information for HR7672A, since the companion is significantly fainter than the primary. It is therefore important to reliably determine the mass of the host star independent of dynamical considerations.

---

[11] This result is consistent with the values (9.94 ± 0.05 mas pixel^{-1} and $0\overset{\circ}{.}0 \pm 0\overset{\circ}{.}5$) provided by the observatory. NIRC2 was not opened nor temperature cycled between 2003 and 2011, including the dates of our imaging observations (R. Campbell 2011, private communication).

[12] We do not include the original Gemini imaging data from 2001 June, which suffers from systematic errors and a low signal-to-noise ratio as described in Liu et al. (2002).

Table 2
The Physical Properties of HR7672A

HR7672A	Value	Technique
θ_{LD} (mas)	0.584 ± 0.010	Interferometry
Radius ($R_\odot$)	1.115 ± 0.021	Interferometry, parallax
Luminosity ($L_\odot$)	1.338 ± 0.032	Spectral energy distribution
T_{eff} (K)	5883 ± 59	Stefan–Boltzmann relation
$\log[R'_{HK}]$	-4.854 ± 0.025	HIRES spectroscopy
V_{macro} (km s^{-1})	4.8	Iterative SME
$V \sin i$ (km s^{-1})	2.1 ± 0.7	Iterative SME
[Fe/H]	0.05 ± 0.07	Iterative SME
$\log g$ (cm s^{-2})	4.42 ± 0.06	Iterative SME
Mass ($M_\odot$)	1.08 ± 0.04	Iterative SME
t_{iso} (Gyr)	2.5 ± 1.8	Iterative SME
t_{gyro} (Gyr)	$2.4^{+0.6}_{-0.7}$	Gyrochronology

Notes. We measure the stellar radius directly using CHARA interferometry. The luminosity is found by fitting a spectral energy distribution from photometry obtained over a broad wavelength range. The effective temperature derived from the Stefan–Boltzmann equation is held fixed as input to SME (sampled separately at $T_{eff} = 5883$ K, $T_{eff} = 5883-59$ K, $T_{eff} = 5883+59$ K). Several SME iterations result in convergence of the stellar surface gravity (log g) between the spectral model and Yonsei-Yale isochrones. The final estimated mass, age, and radius are consistent with the measured stellar luminosity and radius to within 1σ. Our derived stellar mass is also consistent with the model-independent empirical relations of Torres et al. (2010). Our derived stellar age is consistent with the six different age diagnostics of Liu et al. (2002). HR7672A is a G0V star, and thus a convenient calibrator. Its physical properties may be used to infer those of HR7672B, such as metal content and age.

Fortunately, HR7672A is a nearby ($d = 17.77 \pm 0.11$ pc) solar-type (G0V) star, making it possible to (1) measure its radius directly using interferometry and (2) determine its surface gravity from high-resolution spectra using models that are well calibrated from observations of the Sun. We have spatially resolved the surface of HR7672A using the Georgia State University Center for High Angular Resolution astronomy Array (CHARA) (ten Brummelaar et al. 2005). We have also obtained non-iodine (template) spectra of HR7672A for which to model.

In the following, we calculate the mass and age of HR7672A using an iterative version of the Spectroscopy Made Easy (SME) spectral modeling routine (Valenti & Fischer 2005), along with Yonsei-Yale isochrones (Demarque et al. 2004). The models self-consistently incorporate the high-resolution stellar spectrum measured with HIRES, direct stellar radius measured with CHARA, and stellar luminosity determined from an SED. Results for the physical properties of HR7672A, including its radius, luminosity, effective temperature, metallicity, mass, and age are shown in Table 2. Our mass estimate is confirmed using a separate analysis that is model independent and relies only upon the empirical mass–radius relations from Torres et al. (2010). Finally, in addition to an isochronal age, we also calculate the age based on gyrochronology (Mamajek & Hillenbrand 2008).

2.3.1. Stellar Diameter from Interferometry

HR7672 was observed on the nights of 2010 September 18, 19, 2011 August 21, and 2011 October 2, 3 with CHARA at Mount Wilson. We used the CHARA classic beam combiner in H band ($\lambda_{central} = 1.67\,\mu$m) with the longest available baselines, S1E1 (maximum 330 m) and E1W1 (maximum 313 m). Projected baseline lengths ranged between 245 m and 325 m during our observations.
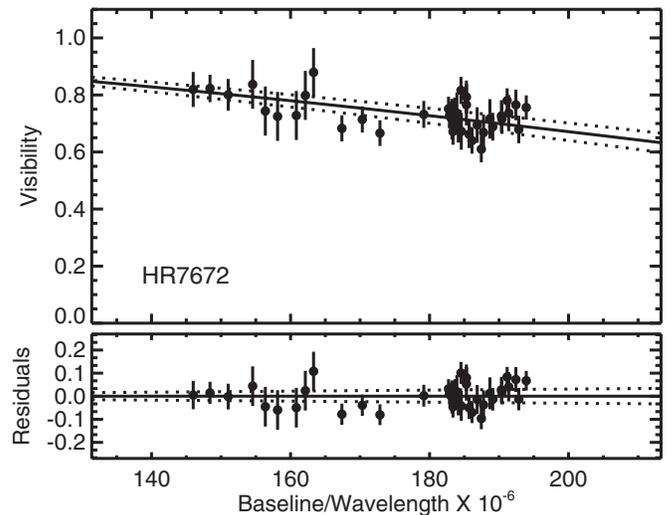
Figure 2. Calibrated visibility measurements and limb-darkened angular diameter fit for HR7672A. Dotted lines indicate the 3σ uncertainty level in the overall fit to the Bessell function. The bottom panel shows the residuals ($\chi_r^2 = 0.5$). Interferometric measurements of the radius of HR7672A allow us to place tight constraints on its mass.

Our observing strategy is analogous to that employed in von Braun et al. (2011a) and von Braun et al. (2011b). We briefly repeat the principle components below. Our interferometric measurements include the common technique of taking bracketed sequences of the object with calibrator stars to characterize and eliminate effects from temporal variations of the atmosphere, telescope, and instrument upon our calculation of interferometric visibilities. We alternate between two nearby calibrators, HD187923 and HD192425, during the observations to minimize systematic errors.

The uniform disk, θ_{UD}, and limb-darkening-corrected, θ_{LD}, diameters[13] are found by fitting our calibrated visibility measurements to the respective functions for each relation. Specifically, we use a linear combination of Bessel functions (Hanbury Brown et al. 1974; Boyajian et al. 2009). Limb-darkening coefficients were taken from Claret (2000). The data and fit for θ_{LD} are shown in Figure 2. The key to understanding the uniqueness of the solution is to recognize that the visibility must approach unity as the baseline approaches zero, and that degeneracies in the slope are broken by the absolute visibility value (as opposed to relative value) for a given baseline, so long as the location along the visibility curve is not mistaken for side lobes in the Bessel function (which effectively corresponds to knowing the distance and luminosity class of the star). Our interferometric measurements yield uniform disk and limb-darkening-corrected angular diameters of $\theta_{UD} = 0.567 \pm 0.010$ mas and $\theta_{LD} = 0.584 \pm 0.010$ mas, respectively. Combined with the *Hipparcos* trigonometric parallax value of $\pi = 56.28 \pm 0.35$ mas (van Leeuwen 2007), we calculate the linear radius of HR7672A to be $R = 1.115 \pm 0.021\,R_\odot$ (Table 2).

2.3.2. Stellar Luminosity and Effective Temperature

Following the procedure outlined in van Belle et al. (2007), we produce a fit to HR7672's SED based on the spectral templates of Pickles (1998) to literature photometry published in the references shown in Table 3. A G0V spectral type provides the best-fitting template. Interstellar extinction is a free

---

[13] The limb-darkening-corrected θ_{LD} corresponds to the angular diameter of the Rosseland, or mean, radiating surface of the star.

Table 3
Literature Photometry for HR7672

Filter	Value (mag)	Reference
Johnson V	5.80 ± 0.05	Johnson et al. (1966)
Johnson B	6.410 ± 0.05	Johnson et al. (1966)
Johnson U	6.500 ± 0.05	Johnson et al. (1966)
Johnson V	5.80 ± 0.05	Cowley et al. (1967)
Johnson B	6.390 ± 0.05	Cowley et al. (1967)
Johnson U	6.500 ± 0.05	Cowley et al. (1967)
Johnson V	5.80 ± 0.05	Johnson & Knuckles (1957)
Johnson B	6.410 ± 0.05	Johnson & Knuckles (1957)
Johnson U	6.500 ± 0.05	Johnson & Knuckles (1957)
Johnson V	5.77 ± 0.05	Niconov et al. (1957)
Johnson B	6.360 ± 0.05	Niconov et al. (1957)
Johnson V	5.79 ± 0.05	Mermilliod (1986)
Johnson B	6.390 ± 0.05	Mermilliod (1986)
Johnson U	6.490 ± 0.05	Mermilliod (1986)
Johnson V	5.799 ± 0.05	Moffett & Barnes (1980)
Johnson B	6.402 ± 0.05	Moffett & Barnes (1980)
Johnson V	5.80 ± 0.05	Nicolet (1978)
Johnson B	6.410 ± 0.05	Nicolet (1978)
Johnson U	6.500 ± 0.05	Nicolet (1978)
Johnson U	6.5 ± 0.05	Barnes et al. (1997)
Johnson U	6.5 ± 0.05	Barnes et al. (1997)
Johnson U	6.53 ± 0.05	Barnes et al. (1997)
Johnson U	6.5 ± 0.05	Barnes et al. (1997)
Johnson U	6.49 ± 0.05	Barnes et al. (1997)
Johnson B	6.41 ± 0.05	Barnes et al. (1997)
Johnson B	6.39 ± 0.05	Barnes et al. (1997)
Johnson B	6.41 ± 0.05	Barnes et al. (1997)
Johnson B	6.41 ± 0.05	Barnes et al. (1997)
Johnson B	6.36 ± 0.05	Barnes et al. (1997)
Johnson B	6.394 ± 0.05	Barnes et al. (1997)
Johnson B	6.39 ± 0.05	Barnes et al. (1997)
Johnson B	6.402 ± 0.05	Barnes et al. (1997)
Johnson V	5.8 ± 0.05	Barnes et al. (1997)
Johnson V	5.8 ± 0.05	Barnes et al. (1997)
Johnson V	5.79 ± 0.05	Barnes et al. (1997)
Johnson V	5.8 ± 0.05	Barnes et al. (1997)
Johnson V	5.77 ± 0.05	Barnes et al. (1997)
Johnson V	5.797 ± 0.05	Barnes et al. (1997)
Johnson V	5.79 ± 0.05	Barnes et al. (1997)
Johnson V	5.799 ± 0.05	Barnes et al. (1997)
Stromgren u	7.681 ± 0.08	Hauck & Mermilliod (1998)
Stromgren v	6.765 ± 0.08	Hauck & Mermilliod (1998)
Stromgren b	6.187 ± 0.08	Hauck & Mermilliod (1998)
Stromgren y	5.80 ± 0.08	Hauck & Mermilliod (1998)
Stromgren u	7.673 ± 0.08	Olsen (1994)
Stromgren v	6.757 ± 0.08	Olsen (1994)
Stromgren b	6.184 ± 0.08	Olsen (1994)
Stromgren y	5.80 ± 0.08	Olsen (1994)
Stromgren u	7.675 ± 0.08	Fabregat & Reglero (1990)
Stromgren v	6.761 ± 0.08	Fabregat & Reglero (1990)
Stromgren b	6.184 ± 0.08	Fabregat & Reglero (1990)
Stromgren y	5.80 ± 0.08	Fabregat & Reglero (1990)
Stromgren u	7.682 ± 0.08	Olsen (1993)
Stromgren v	6.761 ± 0.08	Olsen (1993)
Stromgren b	6.187 ± 0.08	Olsen (1993)
Stromgren y	5.80 ± 0.08	Olsen (1993)
Stromgren u	7.682 ± 0.08	Crawford et al. (1966)
Stromgren v	6.775 ± 0.08	Crawford et al. (1966)
Stromgren b	6.189 ± 0.08	Crawford et al. (1966)
Stromgren y	5.80 ± 0.08	Crawford et al. (1966)
Stromgren u	7.682 ± 0.05	Olsen (1994)
Stromgren u	7.695 ± 0.05	Olsen (1994)
Stromgren u	7.681 ± 0.05	Olsen (1994)
Stromgren u	7.672 ± 0.05	Olsen (1994)
Stromgren b	6.189 ± 0.05	Olsen (1994)

Table 3
(Continued)

Filter	Value (mag)	Reference
Stromgren b	6.204 ± 0.05	Olsen (1994)
Stromgren b	6.186 ± 0.05	Olsen (1994)
Stromgren b	6.183 ± 0.05	Olsen (1994)
Stromgren v	6.775 ± 0.05	Olsen (1994)
Stromgren v	6.781 ± 0.05	Olsen (1994)
Stromgren v	6.76 ± 0.05	Olsen (1994)
Stromgren v	6.756 ± 0.05	Olsen (1994)
Stromgren y	5.8 ± 0.05	Olsen (1994)
Stromgren y	5.82 ± 0.05	Olsen (1994)
Stromgren y	5.799 ± 0.05	Olsen (1994)
Stromgren y	5.799 ± 0.05	Olsen (1994)
Geneva V	5.794 ± 0.08	Rufener (1976)
Geneva V1	6.541 ± 0.08	Rufener (1976)
Geneva B	5.571 ± 0.08	Rufener (1976)
Geneva B1	6.651 ± 0.08	Rufener (1976)
Geneva B2	6.902 ± 0.08	Rufener (1976)
Geneva U	6.888 ± 0.08	Rufener (1976)
Geneva G	6.846 ± 0.08	Rufener (1976)
2Mass K_s	4.388 ± 0.0230	Cutri et al. (2003)
DDO 48	6.017 ± 0.05	McClure & Forrester (1981)
DDO 45	7.02 ± 0.05	McClure & Forrester (1981)
DDO 42	7.643 ± 0.05	McClure & Forrester (1981)
DDO 41	7.658 ± 0.05	McClure & Forrester (1981)
DDO 38	6.863 ± 0.05	McClure & Forrester (1981)
DDO 35	7.767 ± 0.05	McClure & Forrester (1981)

parameter in the fitting process and is calculated to be $A_V = 0.077 \pm 0.017$ mag. The SED fit for HR7672 along with its residuals is shown in Figure 3. We calculate HR7672's stellar bolometric flux to be $F_{BOL} = (1.360 \pm 0.028) \times 10^{-7}$ erg cm^{-2} s^{-1}, and its luminosity to be $L = 1.338 \pm 0.032 \, L_\odot$. Using a rewritten version of the Stefan–Boltzmann law,

$$T_{eff}(\text{K}) = 2341 \left(F_{BOL}/\theta_{LD}^2 \right)^{1/4}, \qquad (1)$$

where F_{BOL} is in units of 10^{-8} erg cm^{-2} s^{-1} and θ_{LD} is in units of mas, we find HR7672 has an effective temperature of $T_{eff} = 5883 \pm 59$ K.

2.3.3. Stellar Surface Gravity, Metallicity, Mass, and Age

Informed by the above results, we use high-resolution spectroscopy, spectral modeling, and stellar isochrones to determine the remaining physical properties of the host star. A template spectrum of HR7672 was obtained with Keck/HIRES ($\lambda/\Delta\lambda = 55,000$) on 2008 September 8. The iodine gas cell was removed from the optical path to isolate the absorption lines of the star. With an integration time of 17 s, we achieved a signal-to-noise ratio of 280 per pixel at 550 nm.

We analyzed the stellar spectrum using the LTE spectral synthesis code SME described in Valenti & Fischer (2005). Recent versions of SME include an iterative scheme that ensures consistency between the surface gravity derived from synthetic spectra and evolutionary models (Valenti et al. 2009). The stellar spectrum is fit using an initial guess for the surface gravity while the effective temperature, metallicity, macroscopic turbulence, and projected rotational velocity are varied to minimize residuals. With each iteration, results are compared to Yonsei-Yale isochrones (Demarque et al. 2004). Model grids are interpolated to yield an estimate for the stellar mass, radius, age, and composition (see Figure 1 of Valenti et al.
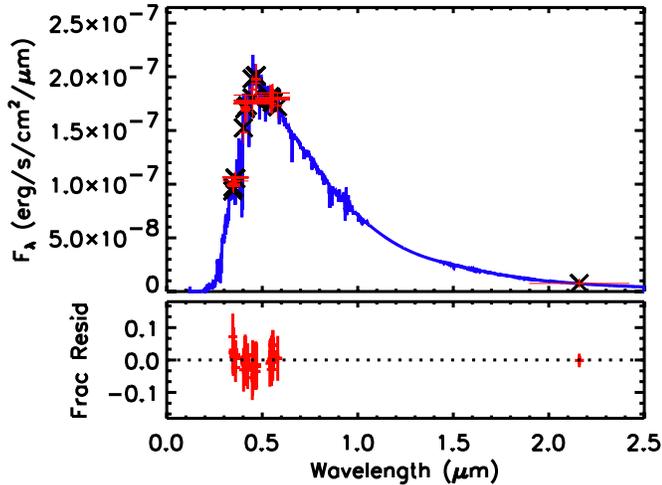
Figure 3. Spectral energy distribution fit for HR7672 ($\chi_r^2 = 0.17$). The (blue) spectrum is a G0V spectral template (Pickles 1998). The (red) crosses indicate photometry values from the literature. "Error bars" in the horizontal direction represent bandwidths of the filters used. The (black) X-shaped symbols show the flux value of the spectral template integrated over the filter transmission. The lower panel displays the residuals around the fit in fractional flux units of photometric uncertainty.

(A color version of this figure is available in the online journal.)

Figure 4. Comparison between a HIRES spectrum (black) and our best-fit SME model (maroon). We use these results along with Yonsei-Yale isochrones to derive the physical properties of HR7672A, self-consistently taking into account independent measurements of the stellar radius from interferometry and luminosity from an SED.

(A color version of this figure is available in the online journal.)

2009). The spectral fitting procedure is repeated using the new (isochronal) surface gravity estimate in the following iteration until the procedure converges—i.e., until the surface gravities agree.

In the case of HR7672, we fit the stellar spectrum by holding $T_{\rm eff}$ fixed, setting it equal to discrete values within the allowable range derived from the Stefan–Boltzmann relation (see Section 2.3.2). Specifically, we analyzed the results for three separate cases: $T_{\rm eff} = T_0$, $T_{\rm eff} = T_0 + \Delta T$, and $T_{\rm eff} = T_0 - \Delta T$, where $T_0 = 5883$ K and $\Delta T = 59$ K (Section 2.3.2). The remaining parameters were varied as usual.[14] We find that the $T_{\rm eff} = T_0 + \Delta T$ case provides the best fit to the HIRES spectrum. It is also the only solution for which the luminosity and radius match the directly measured values to within 1σ (the other cases are consistent to within 2σ).

With this technique, we find a stellar surface gravity, $\log g = 4.42 \pm 0.06$ cm s^{-2}, metallicity, [Fe/H] $= 0.05 \pm 0.07$, mass, $M_* = 1.08 \pm 0.04 \, M_\odot$, and isochronal age, $t_{\rm iso} = 2.5 \pm 1.8$ Gyr. Figure 4 shows a comparison between the HIRES spectrum and our best synthetic model. HR7672's physical properties are listed in (Table 2). Uncertainty in the stellar mass includes propagation of errors from the uncertainty in $T_{\rm eff}$. We adopt this stellar mass for all dynamical calculations.

To further validate our estimate of the host star mass, we use a separate technique that is independent of theoretical spectral and evolutionary models. Torres et al. (2010) have compiled results for dozens of eclipsing binary stars and have constructed a polynomial that relates their measured masses and radii empirically. Using this relation along with the other parameters of HR7672A listed in Table 2, we find that HR7672A has a mass of $M_* = 1.10 \pm 0.04 \, M_\odot$. This result is in agreement with our analysis based on SME and Yonsei-Yale isochrones. Furthermore, the Torres et al. (2010) relations

contain a known bias that systematically overestimates near-solar ($M_* \approx 1.0 \, M_\odot$) stellar masses by as much as $\approx 5\%$. Taking this into account indicates that our above result of $M_* = 1.08 \pm 0.04 \, M_\odot$ is accurate. Finally, we note that our age calculation affirms the original 1–3 Gyr estimate from Liu et al. (2002), which is based on an independent analysis using six different diagnostics, including: comparison of absolute visual magnitude to the location of the main sequence, rotation period, X-ray emission, Ca II H+K emission, kinematics, and lithium absorption. Using the Mamajek & Hillenbrand (2008) empirical relations between rotation period, B−V color, and age, we find a gyrochronological age of $t_{\rm gyro} = 2.4^{+0.6}_{-0.7}$ Gyr, which is also consistent with our isochronal age.

3. JOINT-FIT ORBITAL ANALYSIS

We use Bayesian inference and Markov Chain Monte Carlo (MCMC) simulations to calculate the companion true mass, all six orbital elements, and their uncertainties. The RV and astrometry data are simultaneously fit with a Keplerian orbit. Stellar RV variations, $V_m(t_i)$, are modeled according to

$$V_m(t_j) = K[\cos(\omega + f(t_j)) + e\,\cos(\omega)], \qquad (2)$$

where

$$K = \left(\frac{2\pi G}{P}\right)^{1/3} \frac{m\,\sin(i)}{(1-e^2)^{1/2}(M_* + m)^{2/3}} \qquad (3)$$

is the RV semi-amplitude, ω is the argument of periastron, $f(t_j)$ is the true anomaly at epoch t_j, e is the eccentricity, i is the inclination, P is the orbital period, M_* is the mass of the star, and m is the mass of the companion. Astrometry operates in the orthogonal direction and relates the semimajor axis, a, to the orbital period and system mass through Kepler's equation,

$$P^2 = \frac{4\pi^2 a^3}{G(M_* + m)}, \qquad (4)$$

such that the orbit corresponds to the sky-projected separation of the companion at a given epoch (see Equation (5)) and system parallax.

---

[14] Alternatively, we could set the luminosity and radius input to SME equal to our measured values. By allowing the luminosity and radius to vary, we retain covariance between the parameters and demonstrate that the models naturally reproduce measured values while also accounting for uncertainty in the measurements.

Table 4
RV Offsets and Jitter Values Derived from Our MCMC Analysis
(68.2% Confidence Interval)

Dewar	Telescope	RV Offset (m s^{-1})	RV Jitter (m s^{-1})
6	Lick	⋯	$24.3^{+4.5}_{-5.4}$
8	Lick	$28.4^{+5.5}_{-6.9}$	$9.8^{+1.9}_{-2.7}$
18	Lick	$38.8^{+7.2}_{-8.6}$	$8.5^{+1.4}_{-1.8}$
24	Lick	$63.5^{+9.4}_{-11.4}$	$9.2^{+2.1}_{-2.7}$
39	Lick	$46.9^{+6.0}_{-7.3}$	$9.3^{+1.8}_{-2.3}$
102	Keck	$50.7^{+6.8}_{-8.1}$	$7.1^{+0.9}_{-1.1}$
103	Keck	$65.0^{+10.0}_{-11.9}$	$5.6^{+0.7}_{-0.9}$

The following physical parameters are used as variables in the analysis: the companion period (P), eccentricity (e), inclination (i), argument of periastron (ω), longitude of the ascending node (Ω), time of periastron passage (t_p), and true mass (m). Several nuisance parameters are also required, including differential RV offsets between HIRES and the Hamilton echelle at Lick, to account for the different instrument settings, as well as RV "jitter" to account for astrophysical noise and ensure that the data are weighted properly (Isaacson & Fischer 2010). RV jitter was added directly to the measurement uncertainties, which results in a reduced chi-squared statistic, $\sqrt{\chi_r^2}$, near unity. Given the long time baseline of the observations, a total of six different instrument offsets and seven different jitter terms were required (five from Lick and two from Keck). As expected, the measurement uncertainties decrease with time as well as the relative size of the required jitter, meaning that the RV precision and our ability to estimate the RV precision has improved significantly since 1987 September (Tables 4 and 5).

We use the Metropolis–Hastings algorithm to efficiently explore the multi-dimensional parameter space. A likelihood function, L, self-consistently relates the data, model parameters, and prior information, to the posterior probability density distribution (Ford 2006; Johnson et al. 2011b). The likelihood function used for calculations is given by

$$\ln L = -\sum_{j=1}^{N_{\rm RV}} \ln \sqrt{2\pi(\sigma_j + s_\ell)^2} - \frac{1}{2}\sum_{j=1}^{N_{\rm RV}}\left[\frac{\Delta V(t_j)}{\sigma_j + s_\ell}\right]^2$$
$$-\sum_{k=1}^{N_{\rm Ast}}\left[\ln\sqrt{2\pi\sigma_{X_k}^2} + \ln\sqrt{2\pi\sigma_{Y_k}^2}\right]$$
$$-\frac{1}{2}\sum_{k=1}^{N_{\rm Ast}}\left[\frac{\Delta X(t_k)^2}{\sigma_{X_k}^2} + \frac{\Delta Y(t_k)^2}{\sigma_{Y_j}^2}\right], \quad (5)$$

where $\Delta V(t_j) = V_j - V_m(t_j)$ represents the difference between the RV data and the Keplerian model RV at epoch t_j; $\Delta X(t_k)$ and $\Delta Y(t_k)$ represent the difference in the east and north position of the companion between the astrometric data and the Keplerian model astrometry at epoch t_k, respectively; σ_i and σ_{X_k}, σ_{Y_k} are the individual RV and astrometric uncertainties; and s_ℓ is the RV jitter for instrument setting ℓ (summation over the various instrument settings is implicit). We assume that both the RV and astrometric measurements follow Gaussian distributions.

We randomly select one parameter per MCMC iteration to alter. Candidate transition probability functions follow a normal distribution with adjustable width and are centered on the most recently accepted parameter value. We do not change

Table 5
Doppler Radial Velocity Data

JD−2,440,000	RV (m s^{-1})	Error (m s^{-1})	Instrument	Dewar
7047.7194	270.71	0.81	L	6
7373.8210	232.88	0.38	L	6
7373.9403	222.46	0.68	L	6
7374.8270	208.96	0.63	L	6
7374.9631	241.49	0.87	L	6
7394.7872	223.48	1.29	L	6
7430.6837	260.22	1.02	L	6
7431.6884	273.80	1.10	L	6
7578.0606	247.64	1.29	L	6
7710.8762	232.07	1.29	L	6
7846.7068	201.73	1.03	L	6
8018.9895	191.07	1.64	L	6
8019.9631	216.91	1.63	L	6
8113.8532	150.19	1.02	L	6
8200.6134	176.47	1.03	L	6
8375.0093	158.68	1.63	L	6
8437.9603	173.20	1.53	L	6
8834.8294	133.43	0.75	L	8
8847.8253	128.49	0.93	L	8
8905.7100	136.85	0.84	L	8
9123.0038	91.09	1.38	L	8
9171.8390	103.59	1.11	L	8
9173.8394	98.98	1.26	L	8
9174.9026	110.75	1.12	L	8
9200.8275	100.12	1.04	L	8
9278.7378	105.00	1.08	L	8
9280.7483	97.92	0.99	L	8
9587.7636	80.56	0.98	L	8
9589.7614	82.45	1.03	L	8
9602.7461	101.85	0.96	L	8
9622.7247	90.93	1.26	L	8
9680.5946	66.84	0.76	L	39
9872.9322	54.42	0.49	L	39
9893.8756	61.43	0.50	L	39
9913.9177	45.84	0.51	L	39
9984.6846	56.55	0.51	L	39
10215.8672	8.85	0.78	L	39
10263.8492	26.16	0.54	L	39
10299.8286	33.72	0.61	L	39
10304.8468	18.14	0.56	L	39
10601.8849	0.00	0.01	K	102
10602.9911	3.78	1.29	K	102
10604.0217	3.69	1.19	K	102
10605.0298	2.92	1.30	K	102
10606.0621	−5.73	1.30	K	102
10606.9658	0.77	1.38	K	102
10607.9157	3.79	1.37	K	102
10613.9009	−2.26	0.79	L	39
10614.9313	−0.37	0.75	L	39
10640.8998	6.26	0.75	L	39
10656.8269	7.41	0.76	L	39
10793.5628	1.76	0.51	L	39
10979.9278	−6.21	1.16	L	18
11048.8474	5.92	1.17	L	18
11062.7690	−9.13	1.23	L	18
11068.8450	−23.71	1.45	K	102
11069.8909	−29.20	1.34	K	102
11070.9108	−19.72	1.31	K	102
11071.8471	−13.15	1.60	K	102
11072.8352	−15.16	1.34	K	102
11074.8549	−22.96	1.31	K	102
11075.7848	−22.30	1.18	K	102
11300.0046	−33.20	0.78	L	39
11303.9778	−33.21	0.80	L	18
11305.9730	−32.72	0.88	L	18

Table 5
(Continued)

JD−2,440,000	RV (m s^{-1})	Error (m s^{-1})	Instrument	Dewar
11311.1002	−41.88	1.23	K	102
11312.0886	−40.53	1.37	K	102
11313.1019	−33.60	1.39	K	102
11314.1248	−39.07	1.04	K	102
11367.9059	−53.11	1.51	K	102
11368.8710	−49.16	1.72	K	102
11370.0152	−45.70	1.28	K	102
11372.0268	−41.96	1.64	K	102
11373.0623	−46.15	1.59	K	102
11373.8199	−51.10	1.48	K	102
11389.8655	−51.27	0.80	L	18
11392.8306	−42.50	0.89	L	18
11410.8762	−52.99	1.52	K	102
11411.8717	−55.86	1.39	K	102
11416.7036	−29.17	0.88	L	18
11439.8221	−53.96	1.46	K	102
11467.6397	−28.58	1.57	L	18
11468.6072	−34.72	1.31	L	18
11679.0915	−39.86	1.85	K	102
11703.0748	−46.32	1.50	K	102
11751.8211	−50.03	0.88	L	18
11754.9418	−49.21	1.33	K	102
11793.8250	−53.33	1.63	K	102
11815.6476	−45.26	1.48	L	18
12031.0398	−79.77	1.53	K	102
12041.9946	−78.96	1.22	L	18
12075.9299	−81.23	0.98	L	18
12099.0483	−87.46	1.60	K	102
12115.8858	−87.66	0.95	L	18
12117.8641	−82.71	0.82	L	18
12127.9831	−100.94	1.83	K	102
12133.8002	−98.58	1.62	K	102
12140.7744	−69.50	0.87	L	18
12181.6483	−84.26	0.99	L	18
12186.6687	−75.66	1.15	L	18
12188.7009	−77.17	1.29	L	18
12202.6766	−91.70	1.09	L	18
12391.1392	−120.49	1.91	K	102
12508.7589	−120.32	1.18	L	24
12509.7462	−134.04	1.14	L	24
12515.7825	−115.41	1.12	K	102
12575.6912	−116.79	1.69	K	102
12848.9031	−131.74	1.78	K	102
12855.9988	−136.42	1.67	K	102
12894.7297	−139.06	1.45	L	24
13181.0272	−171.06	1.48	K	102
13203.8281	−160.71	1.90	L	24
13303.7113	−172.17	0.84	K	103
13544.9448	−203.04	1.47	L	24
13551.0081	−195.05	0.55	K	103
13556.9127	−190.72	1.37	L	24
13561.8937	−201.13	1.58	L	24
13589.8255	−186.90	2.81	L	24
13603.9205	−195.75	0.74	K	103
13926.0386	−212.10	0.67	K	103
13926.8957	−217.61	1.65	L	24
13954.7593	−226.25	1.97	L	24
13958.7828	−221.32	1.29	L	24
13982.8138	−220.35	0.62	K	103
13989.8700	−224.79	3.04	L	24
14337.0434	−235.41	1.44	K	103
14546.1518	−240.05	1.22	K	103
14671.9587	−240.90	1.21	K	103
14673.9656	−248.17	1.16	K	103
14675.8841	−247.46	0.93	K	103

Table 5
(Continued)

JD−2,440,000	RV (m s^{-1})	Error (m s^{-1})	Instrument	Dewar
14688.8742	−239.27	1.47	K	103
14689.9519	−241.90	1.36	K	103
14697.9197	−222.74	2.94	L	24
14717.9307	−244.81	1.25	K	103
14718.9864	−246.41	1.27	K	103
14719.9911	−239.01	1.18	K	103
14720.9566	−225.02	1.22	K	103
14721.9701	−218.99	1.19	K	103
14722.8696	−226.22	1.20	K	103
14724.9263	−233.32	1.27	K	103
14725.8416	−232.83	1.23	K	103
14726.9581	−231.17	1.16	K	103
14727.8365	−236.50	1.21	K	103
14777.8159	−235.80	1.43	K	103
14808.7068	−234.60	1.35	K	103
14929.1287	−234.40	1.43	K	103
14930.1221	−237.22	1.34	K	103
14935.1295	−230.98	1.22	K	103
15041.8701	−229.55	1.34	K	103
15076.7430	−230.53	1.29	K	103
15079.7372	−232.51	1.34	K	103
15106.9076	−219.21	1.36	K	103
15169.7567	−230.30	0.88	K	103
15290.1483	−218.21	1.36	K	103
15313.1369	−224.11	1.32	K	103
15319.0997	−226.52	1.48	K	103
15404.9095	−214.63	1.35	K	103
15437.0096	−206.43	1.35	K	103
15542.6875	−198.94	1.15	K	103
15723.0122	−163.58	1.38	K	103
15785.9666	−169.26	1.58	K	103
15842.7963	−158.36	1.57	K	103

Notes. Raw RV measurements used for orbital analysis. Uncertainties correspond to the error due to photon noise only. Observations obtained at Lick and Keck are labeled in the instrument column. Several different hardware configurations have been used over the past 24 years. They are labeled according to dewar number. Each requires different RV offset and jitter values.

the transition function widths following the "burn-in" stage. The algorithm accounts for the covariance between ω and t_p by taking steps in $\omega \pm f_0$, where f_0 is the true anomaly of the companion at the first RV observing epoch. This approach improves the MCMC acceptance rate and accelerates convergence (Ford 2006). We use uniform priors for each parameter. The range of values is, however, truncated to reasonable limits. For example, we only consider companion masses in the range $20 \leqslant m/M_J \leqslant 120$. The eccentricity and other orbit parameters span the full range of possible values.

To identify the global minimum, we compare the results of multiple chains that explore the likelihood manifold starting from different initial states. Convergence is reached once the Gelman–Rubin statistical criterion is met (Gelman & Rubin 1992). Specifically, we require that

$$R(z) = \left(\frac{\bar{S}(z) + M(z)}{\bar{S}(z)} \right)^{1/2} \leqslant 1.1, \qquad (6)$$

for each parameter z, where $\bar{S}(z)$ is the mean of the variance of the MCMC chains, and $M(z)$ is the variance of the mean of
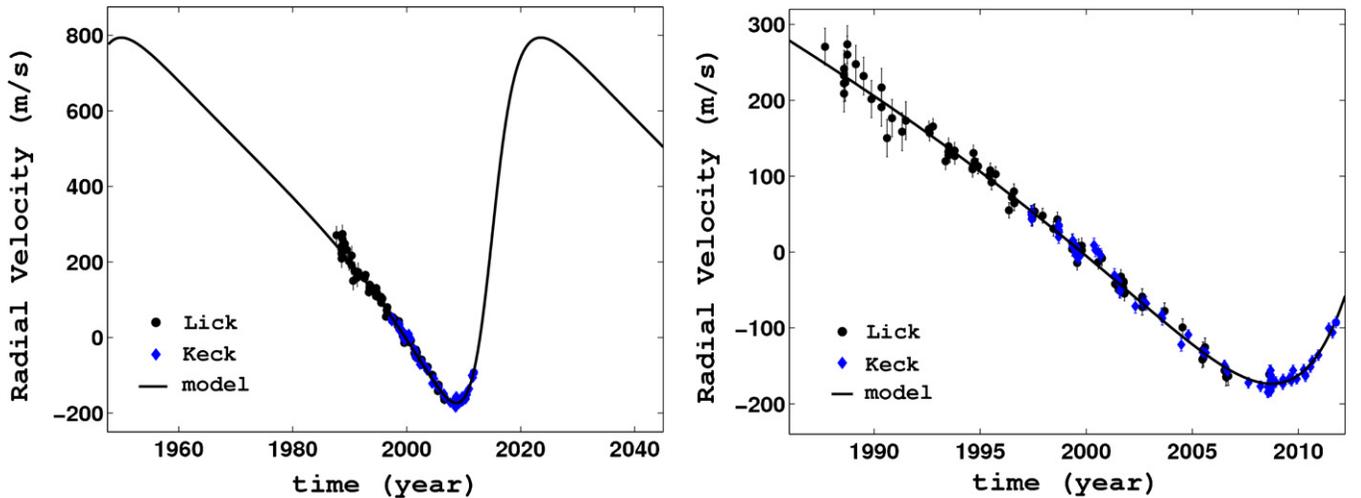
Figure 5. RV data and best-fit model. The Doppler signal shows significant curvature indicative of a high eccentricity. Left: RV time series showing a full predicted orbit cycle. Right: a closer view of the 24 year data set.

(A color version of this figure is available in the online journal.)
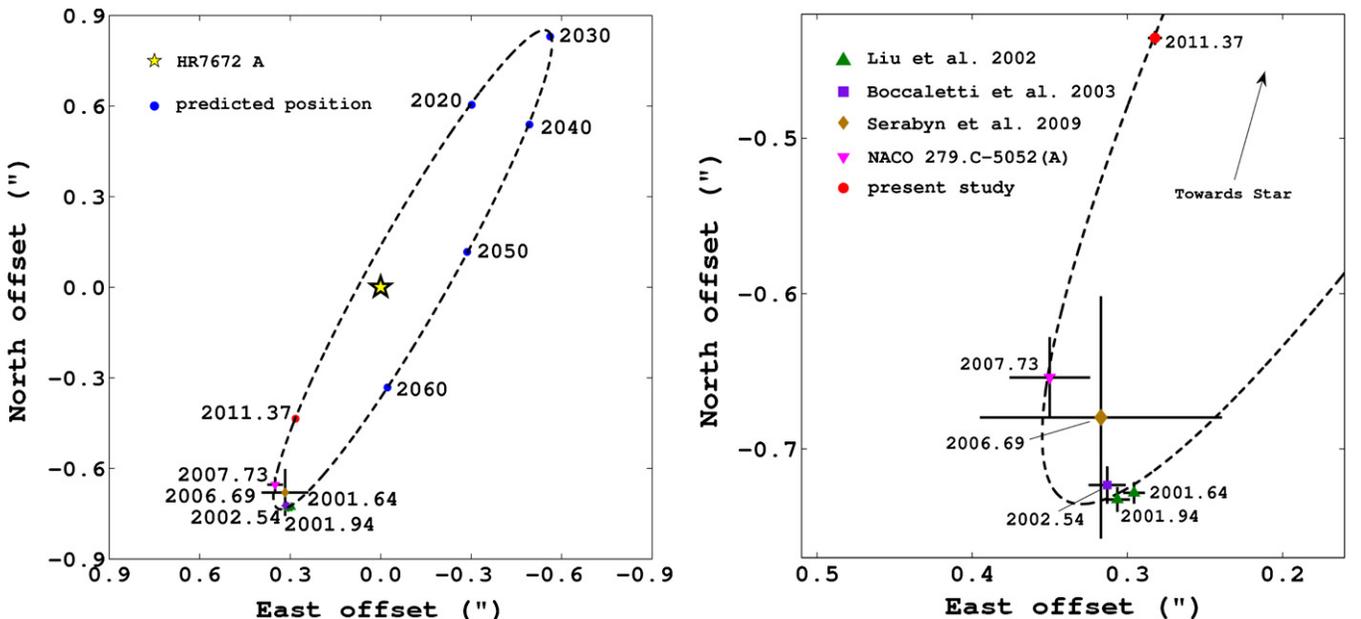
Figure 6. Orbit of HR7672B. Left: full orbit showing recent astrometric measurements (southeast), the best-fit model, and our predictions for where the companion will be located at future epochs (blue dots—dates correspond to September 1). Right: a closer view of the southeast quadrant showing measurements from Liu et al. (2002), Boccaletti et al. (2003), Serabyn et al. (2009), NACO archival data, and our most recent measurement using NIRC2 at Keck, respectively. A much larger plate scale was used for the Serabyn et al. (2009) observations compared to the other studies. The best-fit model passes through the (1σ) error bar of each measurement.

(A color version of this figure is available in the online journal.)

the MCMC chains (see Ford 2006 for details). Following convergence, the individual chains are combined (linked together) to create the final parameter distributions. We find that $\approx 10^8$ iterations are required to provide a sufficiently dense sampling of the posterior distribution.

Uncertainty in the distance to HR7672 is self-consistently folded into the analysis by drawing random distance values from a normal distribution centered on the *Hipparcos* result for each MCMC iteration. The width of the distribution is set to match the measurement error. We account for uncertainty in the mass of the host star in the same way as the uncertainty in the distance, by drawing random stellar mass values from a normal distribution centered on the stellar mass estimate (Section 2.3.3). The results are then combined with the MCMC chains in accordance with the above equations. This technique of incorporating uncertainty

in the distance to HR7672 and the mass of the primary is robust because it preserves the covariance between orbital parameters captured by the MCMC calculations.

4. RESULTS

The RV and astrometry data used in combination with the distance measurement and stellar mass estimate allow the MCMC simulations to consistently converge for each parameter. Only a narrow range of orbital solutions exist that can satisfy the constraints imposed by both data sets simultaneously. Figures 5 and 6 display the final RV and astrometry data along with the best-fit model. The orbit well matches the RV observations and also falls within the (1σ) uncertainty of each astrometric measurement. We find a reduced chi-square, χ_r, value of
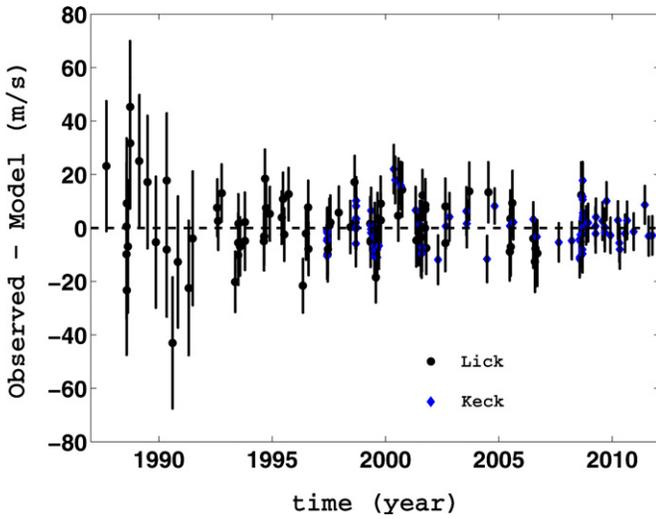
Figure 7. Doppler RV residuals. Precision RV techniques have improved dramatically over the past two decades. In addition to a long time baseline, HR7672 also has many samples per time because it is part of the NASA-UC η-Earth program. Some residual periodicities are noticeable but currently insufficient to claim evidence for the existence of an additional low-mass body with a comparatively short orbital period.

(A color version of this figure is available in the online journal.)

Table 6
Companion Dynamical Mass and Three-dimensional Orbit Parameters Resulting from Our MCMC Analysis

HR7672B	Weighted Mean	68.2% CI	95.4% CI
Mass (M_J)	68.7	65.6–71.1	63.2–74.6
P (year)	73.3	70.4–75.5	68.5–79.0
a (AU)	18.3	17.8–18.7	17.5–19.3
e	0.50	0.49–0.51	0.48–0.52
i (deg)	97.3	96.8–97.7	96.4–98.1
ω (deg)	259	257–261	254–263
Ω (deg)	61.0	60.6–61.3	60.2–61.6
t_p (year)	2014.6	2014.5–2014.7	2014.3–2014.8

Notes. Both 68.2% and 95.4% confidence intervals (CI) are listed. HR7672B is a benchmark brown dwarf with high eccentricity.

Table 7
Apparent Magnitudes of the HR7672 System

Filter	HR7672 A	HR7672 B
V	5.80	$\cdots$
J	4.69	≈ 14.39
H	4.43	14.04 ± 0.14
K	4.49	$K_s = 13.04 \pm 0.10$

Notes. Values for HR7672 A are from SIMBAD. Values for HR7672 B are from Boccaletti et al. (2003).

$\sqrt{\chi_r^2} = 0.96$ per degree of freedom overall. Figure 7 shows the RV residuals following subtraction of our best-fit model from the data.

The final MCMC distributions are shown in Figure 8 and the physical properties of HR7672B are summarized in Table 6; ad-

ditionally, for reference, the apparent magnitudes of HR7672B are shown in Table 7. We find that HR7672B has a high eccentricity, $e = 0.50^{+0.01}_{-0.01}$, and a near edge-on orbit, $i = 97.3^{+0.4}_{-0.5}$ deg.
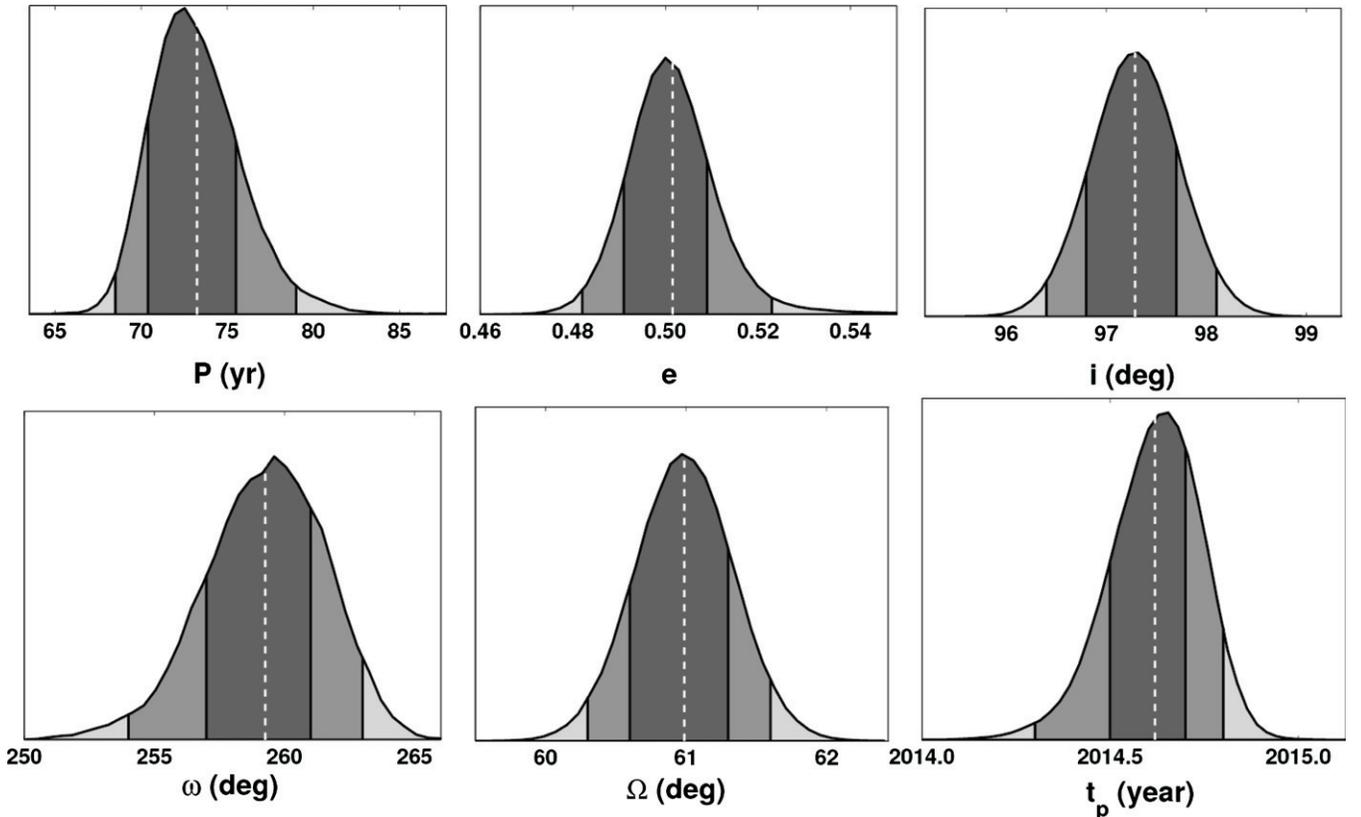
Figure 8. Results from MCMC calculations showing the marginalized posterior distributions of the companion period (P), eccentricity (e), inclination (i), argument of periastron (ω), longitude of the ascending node (Ω), and time of periastron passage (t_p). A vertical dashed line indicates the weighted mean value for each parameter. Shaded regions correspond to 68.2% and 95.4% confidence intervals, respectively.
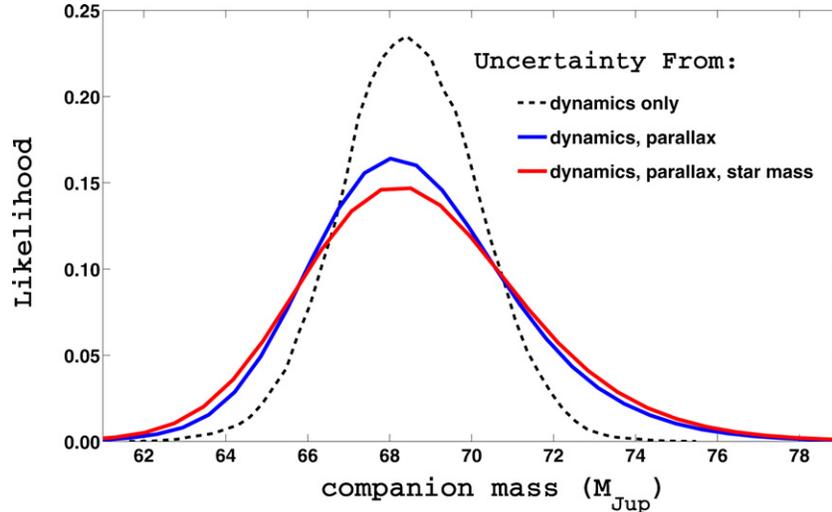
Figure 9. Companion posterior mass distribution shown before and after taking into account uncertainty in the system parallax and mass of the primary star. Uncertainty in the companion mass is limited primarily by having only partial orbital phase coverage.

(A color version of this figure is available in the online journal.)
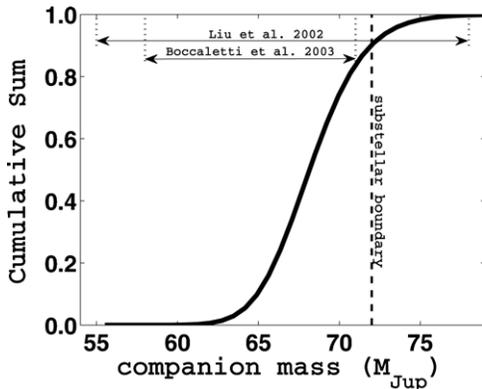
Figure 10. Cumulative summation of the posterior companion mass distribution. The canonical boundary at $72\,M_J$ separating stars from brown dwarfs is labeled for reference. HR7672B is a brown dwarf at 90.1% confidence. Results from orbital dynamics are more accurate and precise than estimates based on spectrophotometry.

It reached greatest elongation (southeast portion of orbit) just following the Liu et al. (2002) direct imaging discovery. The velocity of HR7672B is now increasing sharply as it approaches periastron. Our predictions for its location on September 1 in the years 2020, 2030, 2040, 2050, and 2060 are shown in Figure 6. With an impact parameter of 67 mas, the companion will soon disappear behind the host star, much like the extrasolar planet Beta Pictoris b has evaded detection in the past (Fitzgerald et al. 2009; Lagrange et al. 2010).

We find that HR7672B has a mass of $m = 68.7^{+2.4}_{-3.1}\,M_J$ and thus resides in an interesting regime that borders, but lies just beneath, the hydrogen-fusing limit (Figure 9). Only 9.9% of the distribution lies above the canonical value of $\approx 72\,M_J$, often taken as the dividing line between brown dwarfs and stars (Chabrier et al. 2000). We therefore conclude that HR7672B is a brown dwarf at 90.1% confidence (Figure 10), assuming the companion has the same near-solar metallicity as the primary, which we measure to be [Fe/H] $= 0.05 \pm 0.07$ dex.

Figure 9 also shows the companion mass distribution before and after taking into account the uncertainty in parallax and stellar mass. Uncertainty in the companion mass is limited

primarily by having only a partial orbit, motivating the need for continued Doppler and astrometric monitoring. Uncertainty in parallax is the second largest effect. Significant improvements in parallax over the current *Hipparcos* measurement will likely require dedicated observations from space. Uncertainty in the mass of the primary star is a comparatively small effect, since the companion mass depends weakly upon star mass with Doppler observations. For example, an error of $\pm 0.13\,M_\odot$ in the host star mass would be required to shift the companion mass exterior to its current 95.4% confidence interval. Covariance matrices between the six orbit parameters and the companion mass are shown in Figure 11.

The final companion mass distribution is narrow compared to the range of possible masses resulting from spectrophotometry. For example, Liu et al. (2002) find that the companion has a mass between 55 and 78 M_J, using direct *K*-band spectroscopy, a number of age diagnostics, and the theoretical models of Burrows et al. (1997) and Chabrier et al. (2000). Boccaletti et al. (2003) have obtained complementary photometry in the *J* and *H* bands to refine this estimate. Using the same age range of 1–3 Gyr from Liu et al. (2002), they find that HR7672B has a mass between 58 and 71 M_J. Performing similar calculations with the Baraffe et al. (2003) evolutionary models, we find that HR7672B should have a mass in the 57–74 M_J range. The Baraffe et al. (2003) models are in excellent agreement with the more recent Saumon & Marley (2008) models for L dwarfs older than several Myr. Thus, in each case our calculations using orbital dynamics are already more precise and accurate than estimates based on analyzing light received directly from the companion (Figure 10).

5. SUMMARY AND DISCUSSION

We present the first three-dimensional orbit solution and mass determination for a directly imaged L-dwarf companion to a solar-type star. HR7672 is a unique benchmark system because (1) the primary is a G0V star amenable to ultra-precise Doppler measurements, (2) the metallicity of the primary is reliably determined from spectroscopy, (3) the mass and age of the primary are well constrained, and (4) the parallax has been measured with a fractional error of only 0.6%.
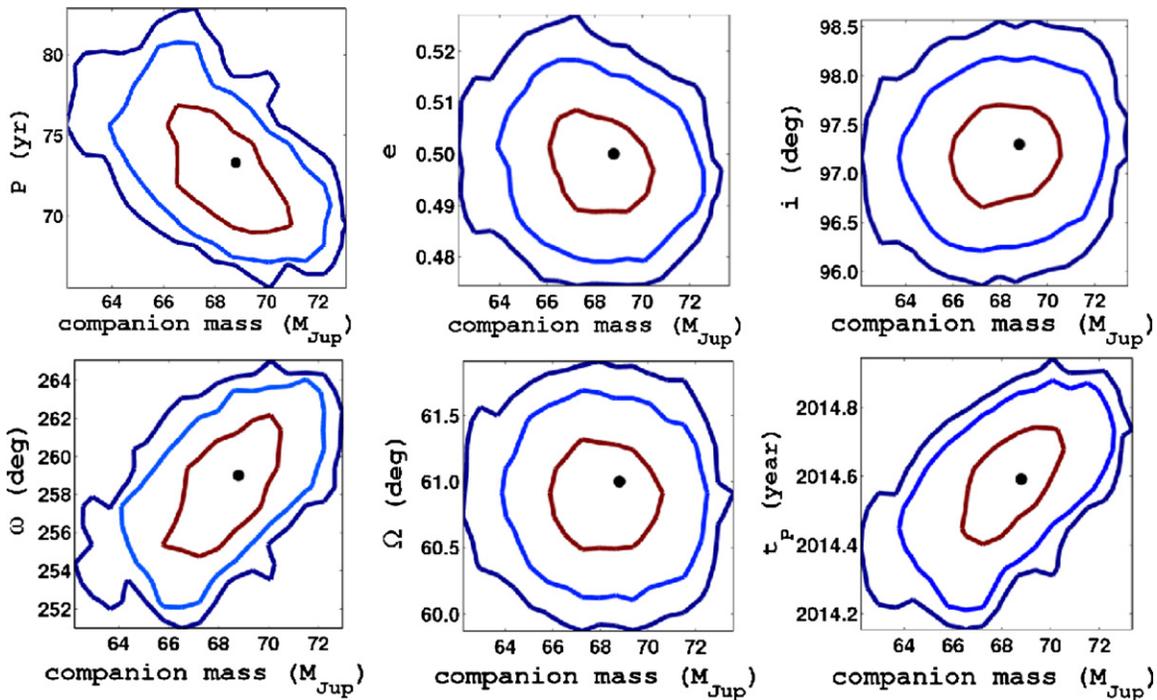
Figure 11. Probability matrices showing the covariance between the companion mass and all six orbital elements. Each panel shows the posterior distribution of two parameters marginalized over the remaining variables including RV offsets and jitter. The contours indicate iso-probability levels corresponding to 68.2% (red), 95.4% (light blue), and 99.7% (dark blue), respectively, prior to accounting for uncertainty in the system parallax and star mass. A black circle denotes the best-fit values. The companion mass is strongly covariant with the orbital period and argument of periastron (and likewise time of periastron passage).

(A color version of this figure is available in the online journal.)

We have monitored HR7672 with precise RV measurements for 24 years, covering 33% of an orbital cycle. The observational cadence is high compared to other trend stars because this system was also a target of the NASA-UC η-Earth program (Howard et al. 2010), which began conveniently around the same time as the Doppler signal started to show curvature. We have also obtained a recent high-contrast image of the system with NIRC2 at Keck, significantly increasing the astrometric time baseline by extending the sky-projected orbital coverage to 13% of a full cycle. Both data sets have a high ($\approx$100) signal-to-noise ratio and exhibit substantial orbital motion. We have performed a joint Doppler-astrometric MCMC analysis to compute the companion orbital elements, true mass, and their uncertainties.

We find that HR7672B has a near edge-on, $i = 97.3^{+0.4}_{-0.5}$ deg, highly eccentric, $e = 0.50^{+0.01}_{-0.01}$, orbit, with a semimajor axis of $a = 18.3^{+0.4}_{-0.5}$ AU. Presently accelerating on its path back toward the primary star, both from the perspective of the Earth and from the perspective of HR7672A, this companion will gradually becoming more difficult to image directly. We predict that HR7672B will reach periastron in the year 2014, just prior to disappearing behind HR7672A. This companion does not yet have JH spectra. We recommend that high-contrast imaging programs employing integral-field spectrographs observe this target as soon as possible, while the components are reasonably well separated.

The mass of HR7672B is $68.7^{+2.4}_{-3.1}$ M_J. This L4.5 ± 1.5 dwarf therefore resides near the stellar/substellar boundary, though is likely a brown dwarf if not a transition object: 90.1% of the mass probability distribution falls below the $72 M_J$ dividing line. Our dynamical measurement is more accurate and precise than that obtained previously from spectrophotometry and the use of theoretical models. With a fractional error of only 4%, it is comparable to the results for transiting brown dwarfs (Stassun

et al. 2006; Johnson et al. 2011a). Uncertainty in the mass will decrease further as additional RV and astrometric measurements are obtained.

These observations provide a mass determination that is completely independent of the companion spectrum, colors, and luminosity (see Appendix A for an estimate of the companion bolometric luminosity). Presently, few benchmark systems have dynamical mass measurements and provide such comprehensive information. For instance, GD165B has been well characterized with optical and near-infrared spectroscopy, but its age is uncertain because it orbits a white dwarf (Kirkpatrick et al. 1999a; Jones et al. 1994). HD203030B has also been studied across a wide bandpass, conveniently orbits a G8V star, and has a narrow age range (130–400 Myr), but its projected separation is 487 AU, thus prohibiting a dynamical mass (Metchev & Hillenbrand 2006). Likewise, HD3651B and HD114762B orbit solar-type stars but their projected separations are 480 AU and 128 AU, respectively (Liu et al. 2007; Bowler et al. 2009). Many other dynamical measurements have targeted companions to M-stars, thus helping to circumvent issues with contrast (Zapatero Osorio et al. 2004; Ireland et al. 2008; Dupuy et al. 2009b; Konopacky et al. 2010), but M-star metallicities are notoriously difficult to determine (Johnson & Apps 2009). Low-mass companions to solar-type stars have also been studied using Doppler measurements in combination with *Hubble Space Telescope* astrometry (Benedict et al. 2010) and *Hipparcos* intermediate astrometry (Sahlmann et al. 2011), but indirect observations preclude a comparison between spectral models and dynamical mass measurements by definition. One comparable system, HD130948BC, consists of a double brown dwarf orbiting a G2V primary. Although RVs have not been obtained for the pair, which are nominally separated by $\approx$100 mas, a near-unity luminosity ratio permits a precise individual mass

determination (Dupuy et al. 2009a; Konopacky et al. 2010). We conclude that HR7672B is thus a rare and precious mass, age, and metallicity benchmark brown dwarf companion that may be used to explicitly calibrate theoretical evolutionary models and synthetic spectral models by anchoring input parameters to measured values.

Detailed substellar companion characterization studies are particularly relevant now that the first extrasolar planet spectra are securely in hand (Bowler et al. 2010; Barman et al. 2011a, 2011b). As the next generation of high-contrast imaging instruments come online (e.g., Hinkley et al. 2011), and more cold bodies orbiting nearby stars are discovered, HR7672B will serve as a helpful guide for the development of more sophisticated theoretical models by providing a link between our understanding of stars and planets.

APPENDIX A

THE LUMINOSITY OF HR7672B

We can estimate the luminosity of HR7672B using its apparent magnitude and parallax by applying a near-infrared bolometric correction derived from M, L, and T field dwarfs.

The apparent magnitudes of HR7672B are measured to be $m_J \approx 14.39 \pm 0.20$, $m_H = 14.04 \pm 0.14$, and $m_{K_s} = 13.04 \pm 0.10$ (Boccaletti et al. 2003). Of these, the K-band magnitude is regarded as most reliable, given the contrast ratio between the companion and host star. We recalculate the absolute magnitude from Boccaletti et al. (2003), owing to the revised *Hipparcos* parallax since the time of publication, finding $M_{K_s} = 11.79 \pm 0.10$. Liu et al. (2002) arrive at a similar answer of $M_{K_s} = 11.8 \pm 0.1$ using relations between spectral type and absolute magnitudes from Kirkpatrick et al. (2000).

To calculate a bolometric magnitude, we next derive an estimate for the bolometric correction using the empirical relations from Golimowski et al. (2004). Correcting for the expected change in magnitude between the K_s filter and K filter, which results in an ≈ 0.11 mag increase in brightness (i.e., Rudy et al. 1996), and using a spectral type of L4.5, we find $BC_K = 3.35 \pm 0.13$, where the uncertainty is given by the rms scatter in the polynomial fit. The bolometric magnitude is thus

$$M_{\rm BOL} = M_K + {\rm BC}_K = 15.05 \pm 0.23. \qquad (A1)$$

Using the Sun as a reference with $M_{\rm BOL,\odot} = 4.74$, we find that the luminosity of HR7672B is equal to $L = (7.5 \pm 1.6) \times 10^{-5} L_\odot$. With an age of $t_{\rm gyro} = 2.4^{+0.6}_{-0.7}$ Gyr, this result appears to be inconsistent with theoretical cooling models which under-predict its luminosity by a factor of ≈ 2 (Burrows et al. 1997; Baraffe et al. 2003). Applying the Stefan–Boltzmann equation, we estimate the radius to be $R \approx 1.0 \pm 0.4 R_J$, assuming an effective temperature in the middle of the 1510–1850 K range found by Liu et al. (2002).

APPENDIX B

THE SPIN AXIS OF HR7672A

We can also estimate the inclination of the primary star rotation axis. Modeling of HR7672A's spectrum yields a projected rotational velocity of $V \sin i = 2.1 \pm 0.7$ km s^{-1}. Using our measurement of $\log R'_{HK} = -4.854 \pm 0.025$ for the chromospheric Ca II H and K emission, we employ the Noyes et al. (1984) empirical relations to estimate the rotational period, $P_{\rm rot}$. With $B - V = 0.61$ and a convective turnover time of $\log(\tau/{\rm days}) = 0.99 \pm 0.06$, we find $P_{\rm rot} = 17.5 \pm 2.3$ days, assuming a mixing length to scale height ratio of 1.9 (see Wright et al. 2004 and Noyes et al. 1984, and references therein for details). Combining this result with our direct radius measurement (Section 2.3.1), we find that the inclination of the stellar rotation axis is $i_{\rm rot} = 39^\circ \pm 16^\circ$, where $i_{\rm rot} = 0$ corresponds to a pole-on orientation. Thus, the spin axis of HR7672A and the orbit of HR7672B are *not* aligned.

REFERENCES

Absil, O., & Mawet, D. 2010, A&AR, 18, 317
Aitken, R. G. 1919, PASP, 31, 196
Allard, F., Hauschildt, P. H., Alexander, D. R., & Starrfield, S. 1997, ARA&A, 35, 137
Baraffe, I., Chabrier, G., Barman, T. S., Allard, F., & Hauschildt, P. H. 2003, A&A, 402, 701
Barman, T. S., Macintosh, B., Konopacky, Q. M., & Marois, C. 2011a, ApJ, 733, 65
Barman, T. S., Macintosh, B., Konopacky, Q. M., & Marois, C. 2011b, ApJ, 735, L39
Barnes, T. G., III, Fernley, J. A., Frueh, M. L., et al. 1997, PASP, 109, 645
Basri, G., Marcy, G. W., & Graham, J. R. 1996, ApJ, 458, 600
Becklin, E. E., & Zuckerman, B. 1988, Nature, 336, 656
Benedict, G. F., McArthur, B. E., Bean, J. L., et al. 2010, AJ, 139, 1844

Bernstein, G., & Khushalani, B. 2000, AJ, 120, 3323
Biller, B. A., Liu, M. C., Wahhaj, Z., et al. 2010, ApJ, 720, L82
Boccaletti, A., Chauvin, G., Lagrange, A.-M., & Marchis, F. 2003, A&A, 410, 283
Boden, A. F., Torres, G., & Latham, D. W. 2006, ApJ, 644, 1193
Bowler, B. P., Johnson, J. A., Marcy, G. W., et al. 2010, ApJ, 709, 396
Bowler, B. P., Liu, M. C., & Cushing, M. C. 2009, ApJ, 706, 1114
Boyajian, T. S., McAlister, H. A., Cantrell, J. R., et al. 2009, ApJ, 691, 1243
Burrows, A., Marley, M., Hubbard, W. B., et al. 1997, ApJ, 491, 856
Burrows, A., Sudarsky, D., & Hubeny, I. 2006, ApJ, 640, 1063
Butler, R. P., Marcy, G. W., Williams, E., et al. 1996, PASP, 108, 500
Chabrier, G., Baraffe, I., Allard, F., & Hauschildt, P. 2000, ApJ, 542, 464
Claret, A. 2000, A&A, 363, 1081
Close, L. M., Lenzen, R., Guirado, J. C., et al. 2005, Nature, 433, 286
Cowley, A. P., Hiltner, W. A., & Witt, A. N. 1967, AJ, 72, 1334
Crawford, D. L., Barnes, J. V., Faure, B. Q., & Golson, J. C. 1966, AJ, 71, 709
Crepp, J. R., Pueyo, L., Brenner, D., et al. 2011, ApJ, 729, 132
Cumming, A., Marcy, G. W., & Butler, R. P. 1999, ApJ, 526, 890
Currie, T., Thalmann, C., Matsumura, S., et al. 2011, ApJ, 736, L33
Cushing, M. C., Kirkpatrick, J. D., Gelino, C. R., et al. 2011, ApJ, 743, 50
Cushing, M. C., Marley, M. S., Saumon, D., et al. 2008, ApJ, 678, 1372
Cutri, R. M., Skrutskie, M. F., van Dyk, S., et al. 2003, 2MASS All Sky Catalog of Point Sources
Demarque, P., Woo, J.-H., Kim, Y.-C., & Yi, S. K. 2004, ApJS, 155, 667
Dupuy, T. J., & Liu, M. C. 2011, ApJ, 733, 122
Dupuy, T. J., Liu, M. C., & Ireland, M. J. 2009a, ApJ, 692, 729
Dupuy, T. J., Liu, M. C., & Ireland, M. J. 2009b, ApJ, 699, 168
Fabregat, J., & Reglero, V. 1990, A&AS, 82, 531
Fitzgerald, M. P., Kalas, P. G., & Graham, J. R. 2009, ApJ, 706, L41
Ford, E. B. 2006, ApJ, 642, 505
Galicher, R., Marois, C., Macintosh, B., Barman, T., & Konopacky, Q. 2011, ApJ, 739, L41
Gelman, A., & Rubin, D. B. 1992, Statistical Science, 7, 457
Ghez, A. M., Salim, S., Weinberg, N. N., et al. 2008, ApJ, 689, 1044
Golimowski, D. A., Leggett, S. K., Marley, M. S., et al. 2004, AJ, 127, 3516
Hanbury Brown, R., Davis, J., Lake, R. J. W., & Thompson, R. J. 1974, MNRAS, 167, 475
Hauck, B., & Mermilliod, M. 1998, A&AS, 129, 431
Hayward, T. L., Brandl, B., Pirger, B., et al. 2001, PASP, 113, 105
Hinkley, S., Oppenheimer, B. R., Zimmerman, N., et al. 2011, PASP, 123, 74
Howard, A. W., Marcy, G. W., Johnson, J. A., et al. 2010, Science, 330, 653
Ireland, M. J., Kraus, A., Martinache, F., Lloyd, J. P., & Tuthill, P. G. 2008, ApJ, 678, 463
Isaacson, H., & Fischer, D. 2010, ApJ, 725, 875
Janson, M., Carson, J., Thalmann, C., et al. 2011, ApJ, 728, 85
Johnson, H. L., & Knuckles, C. F. 1957, ApJ, 126, 113
Johnson, H. L., Mitchell, R. I., Iriarte, B., & Wisniewski, W. Z. 1966, Commun. Lunar Planet. Lab., 4, 99
Johnson, J. A., & Apps, K. 2009, ApJ, 699, 933
Johnson, J. A., Apps, K., Gazak, J. Z., et al. 2011a, ApJ, 730, 79
Johnson, J. A., Clanton, C., Howard, A. W., et al. 2011b, ApJS, 197, 26
Jones, H. R. A., Longmore, A. J., Jameson, R. F., & Mountain, C. M. 1994, MNRAS, 267, 413
Kirkpatrick, J. D., Allard, F., Bida, T., et al. 1999a, ApJ, 519, 834
Kirkpatrick, J. D., Reid, I. N., Liebert, J., et al. 1999b, ApJ, 519, 802
Kirkpatrick, J. D., Reid, I. N., Liebert, J., et al. 2000, AJ, 120, 447
Konopacky, Q. M., Ghez, A. M., Barman, T. S., et al. 2010, ApJ, 711, 1087

Lafrenière, D., Marois, C., Doyon, R., Nadeau, D., & Artigau, É. 2007, ApJ, 660, 770
Lagrange, A., Bonnefoy, M., Chauvin, G., et al. 2010, Science, 329, 57
Lane, B. F., Zapatero Osorio, M. R., Britton, M. C., Martín, E. L., & Kulkarni, S. R. 2001, ApJ, 560, 390
Liu, M. C., Delorme, P., Dupuy, T. J., et al. 2011, ApJ, 740, 108
Liu, M. C., Fischer, D. A., Graham, J. R., et al. 2002, ApJ, 571, 519
Liu, M. C., Leggett, S. K., & Chiu, K. 2007, ApJ, 660, 1507
Lu, J. R., Ghez, A. M., Hornstein, S. D., et al. 2009, ApJ, 690, 1463
Luhman, K. L., Burgasser, A. J., & Bochanski, J. J. 2011, ApJ, 730, L9
Mamajek, E. E., & Hillenbrand, L. A. 2008, ApJ, 687, 1264
Marcy, G. W., & Butler, R. P. 1992, PASP, 104, 270
Marley, M. S., Saumon, D., & Goldblatt, C. 2010, ApJ, 723, L117
Marley, M. S., Seager, S., Saumon, D., et al. 2002, ApJ, 568, 335
Marois, C., Lafrenière, D., Doyon, R., Macintosh, B., & Nadeau, D. 2006, ApJ, 641, 556
McClure, R. D., & Forrester, W. T. 1981, Publ. Dom. Astrophys. Obs. Victoria, 15, 439
Mermilliod, J.-C. 1986, Catalogue of Eggen's UBV Data, 0
Metchev, S. A., & Hillenbrand, L. A. 2006, ApJ, 651, 1166
Moffett, T. J., & Barnes, T. G., III 1980, ApJS, 44, 427
Nakajima, T., Oppenheimer, B. R., Kulkarni, S. R., et al. 1995, Nature, 378, 463
Nicolet, B. 1978, A&AS, 34, 1
Niconov, V. B., Nekrasova, S. V., Polosuina, N. S., Rachkouvsky, N. D., & Chuvajev, W. K. 1957, Izv. Ordena Tr. Krasnogo Znameni Krym. Astrofiz. Obs., 17, 42
Noyes, R. W., Hartmann, L. W., Baliunas, S. L., Duncan, D. K., & Vaughan, A. H. 1984, ApJ, 279, 763
Olsen, E. H. 1993, A&AS, 102, 89
Olsen, E. H. 1994, A&AS, 106, 257
Oppenheimer, B. R., & Hinkley, S. 2009, ARA&A, 47, 253
Oppenheimer, B. R., Kulkarni, S. R., Matthews, K., & Nakajima, T. 1995, Science, 270, 1478
Pickles, A. J. 1998, PASP, 110, 863
Pinfield, D. J., Jones, H. R. A., Lucas, P. W., et al. 2006, MNRAS, 368, 1281
Rebolo, R., Zapatero Osorio, M. R., & Martín, E. L. 1995, Nature, 377, 129
Rudy, R. J., Rossano, G. S., & Puetter, R. C. 1996, ApJ, 458, L41
Rufener, F. 1976, A&AS, 26, 275
Sahlmann, J., Lovis, C., Queloz, D., & Ségransan, D. 2011, A&A, 528, L8
Saumon, D., & Marley, M. S. 2008, ApJ, 689, 1327
Serabyn, E., Mawet, D., Bloemhof, E., et al. 2009, ApJ, 696, 40
Stassun, K. G., Mathieu, R. D., & Valenti, J. A. 2006, Nature, 440, 311
Stevenson, D. J. 1991, ARA&A, 29, 163
ten Brummelaar, T. A., McAlister, H. A., Ridgway, S. T., et al. 2005, ApJ, 628, 453
Torres, G., Andersen, J., & Giménez, A. 2010, A&A, 18, 67
Valenti, J. A., Fischer, D., Marcy, G. W., et al. 2009, ApJ, 702, 989
Valenti, J. A., & Fischer, D. A. 2005, ApJS, 159, 141
van Belle, G. T., Ciardi, D. R., & Boden, A. F. 2007, ApJ, 657, 1058
van Leeuwen, F. 2007, A&A, 474, 653
Vogt, S. S., Allen, S. L., Bigelow, B. C., et al. 1994, Proc. SPIE, 2198, 362
von Braun, K., Boyajian, T. S., Kane, S. R., et al. 2011a, ApJ, 729, L26
von Braun, K., Boyajian, T. S., ten Brummelaar, T. A., et al. 2011b, ApJ, 740, 49
Wahhaj, Z., Liu, M. C., Biller, B. A., et al. 2011, ApJ, 729, 139
Wright, J. T., Marcy, G. W., Butler, R. P., & Vogt, S. S. 2004, ApJS, 152, 261
Zapatero Osorio, M. R., Lane, B. F., Pavlenko, Y., et al. 2004, ApJ, 615, 958